

AERODYNAMIC FEASIBILITY OF A NOVEL SWIVEL ROTOR ARCHITECTURE

Bambang I. Soemarwoto[1]

[1]Royal Netherlands Aerospace Centre NLR, Anthony Fokkerweg 2, 1059 CM Amsterdam, The Netherlands

Abstract

A novel swivel rotor architecture aimed for high performance on all flight regimes (hover, VTOL and high-speed cruise) is presented. It features rotating blades attached on a ring with a large radius. The ring swivels from a horizontal to a vertical position, changing the flight mode from hover to cruise. CFD results highlighting the aerodynamic potentials of the new architecture are presented.

Keywords: rotorcraft, rotor optimization, VTOL, silent rotor

1. Introduction

Due to pressing demands to reduce emissions of carbon and NOx, there is a growing interest in new types of propulsion that offer solutions for a wide range of applications. Novel configurations are emerging such as new concepts of high-speed helicopters, electrical aircraft with distributed propulsion and commercial drones. A novel swivel rotor architecture is introduced in this paper, which is expected to deliver high performance on all modes of flight: hover, VTOL and high-speed cruise.

The objective of the paper is to present an early quantification of the aerodynamic potentials of the swivel rotor architecture by means of a high-fidelity Computational Fluid Dynamics (CFD) method. For a flight mode, an assessment will be presented in terms of lift and drag of the fuselage along with the thrust and power of the rotor. A preliminary evaluation of the noise is also presented.

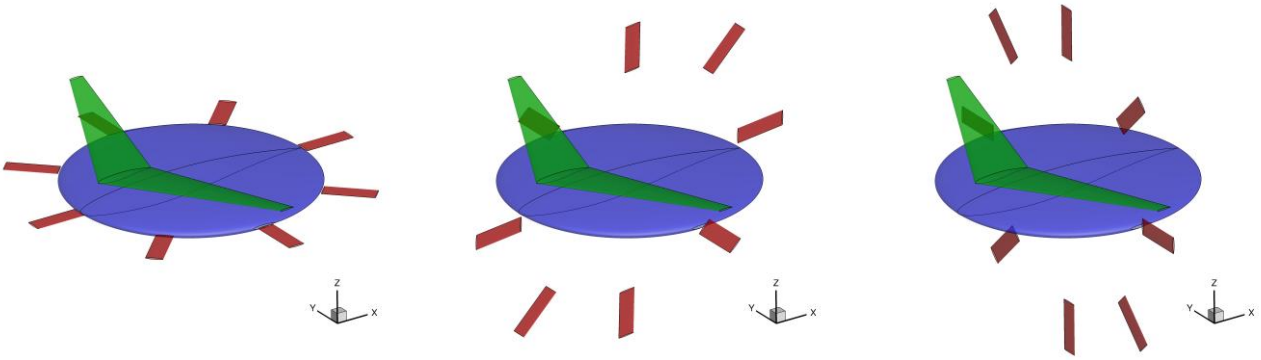
The paper is organized as follows. Section 2 presents a schematic representation of the aircraft explaining how an aircraft with a swivel rotor configuration operates. Section 3 defines a specific realistic use-case in order to determine relevant requirements for a high-speed heavy-lift drone, in terms of weight, volume, speed and altitude. Section 4 describes a model swivel rotor configuration consisting of a fuselage and rotor. Considerations for the selection of the geometries of the fuselage and rotor are presented. A transformation procedure from a conventional to a swivel configuration of the rotor is explained, and a parameterization scheme for the generation of the fuselage and rotor geometries is described. Section 5 briefly describes the CFD method used in this study. Section 6 presents an analysis of the impacts of a swivel rotor configuration with respect to the conventional one. Section 7 summarizes a design for purpose exercise that utilizes the swivel rotor architecture. Section 8 presents a preliminary assessment of the noise, and finally in Section 9 conclusions and recommendations are provided.

2. Architecture

A schematic of an aircraft with a swivel rotor configuration is presented in Figure 1. In this illustration, it consists of three components: fuselage, wing and rotor blades. All components have an airfoil cross-section such that the fuselage also generates lift. In this respect, the wing may be optional depending on whether or not the fuselage can generate a sufficient lift at cruise.

Imagine the rotating blades are attached on a ring at a large radius from the rotation axis. The ring can swivel from a horizontal to a vertical position, back and forth. In the horizontal position, the blades function as a rotor in a hover or VTOL flight mode, producing thrust in the vertical direction to carry the weight. As the ring swivels from the horizontal to the vertical position in a transition flight

mode, the aircraft gains altitude and speed. During this transitional flight mode from hover to cruise, the role of carrying the weight is shifted from the propeller to the fuselage. In the vertical position, the blades will function as a propeller in a high-speed cruise, producing thrust in the flight direction, where both the wing and fuselage will generate lift by virtue of the speed.



(a) take-off (b) transition (c) cruise

Figure 1 – Schematic of the swivel rotor configuration.

Aerodynamic advantages are expected due to (i) low interferences between the blades and the other components in particular in a high-speed cruise, (ii) the number of blades is not limited by the diameter of a hub as in the conventional propeller situation, and (iii) the large radius of the rotation makes the incoming flow fairly uniform along the blade span, as such that there is no need for a strong twist variation that is inevitable in the case of a conventional propeller. There is a high degree of freedom to adjust the number of blades in order to meet a thrust and weight requirement. A significant difference in the noise signature can also be expected due to a lower rotational speed for the same blade tip speed of a conventional propeller.

3. Use Case and Mission

A high-speed heavy-lift drone for medical emergency missions is defined as a use-case to examine the aerodynamic feasibility of the swivel rotor configuration. A case in Indonesia is considered, where the statistics show that it has a relatively high number of stroke events. In a population of 285 million, stroke is the number one leading cause of death, with an incidence rate of 158 stroke events per 100,000 population per year [1]. This corresponds to about half a million new cases annually. The diagnosis of the type of stroke is essential for the determination of the medical treatment. There are two types of strokes, ischemic and hemorrhage, for which the medical treatments are opposites. While the cycle from admission to diagnosis and treatment must be as quick as possible to be within the golden hour to increase the chance of survival, a wrong diagnosis may substantially worsen the patient's condition.

Essential to the diagnosis of stroke is a Magnetic Resonance Imaging (MRI) equipment to scan the brain. The current standard is based on a large facility with a 3 Tesla magnetic field, which has to be specially constructed in a shielded room inside a hospital. An emerging technology uses a low magnetic field of less than 0.1 Tesla, using a light weight array of permanent magnets. The low-field MRI system can be powered by a normal wall socket, which makes it affordable and mobile. With a weight of about 200 kg and a cylindrical volume of 1.8 m^3, illustrated in Figure 2, it can practically be brought to the location of the patient as a point-of-care (POC) medical system [2].



Figure 2 – Magnet array of a low-field MRI (courtesy of Open Imaging B.V).

Indonesia is a vast archipelagic country covering a total of 17,000 islands, of which 6,000 islands are inhabited. Figure 3 presents a distribution of the stroke incidence across Indonesia. The frontline medical care in Indonesia is given by about 10,000 Community Health Centers, distributed in the country as shown in Figure 4. Regions with a high stroke incidence rate are not necessarily the ones with the most underserved communities in terms of population per center. However, if population densities and geographical characteristics are taken into account, access to primary health care may be most challenging to communities in coastal areas. About 60% of the population (170 million people) live in coastal areas [3]. For them, the vast water bodies of the sea form a significant barrier.

The above observation defines the mission of the high-speed heavy-lift drone: “to transport a 200 kg payload of such a cylindrical volume across the sea for a distance of a few hundred kilometers, within a shortest possible time, in order to pursue the golden hour and ensure an effective point-of-care medical system for stroke patients in the nearest community health center”.

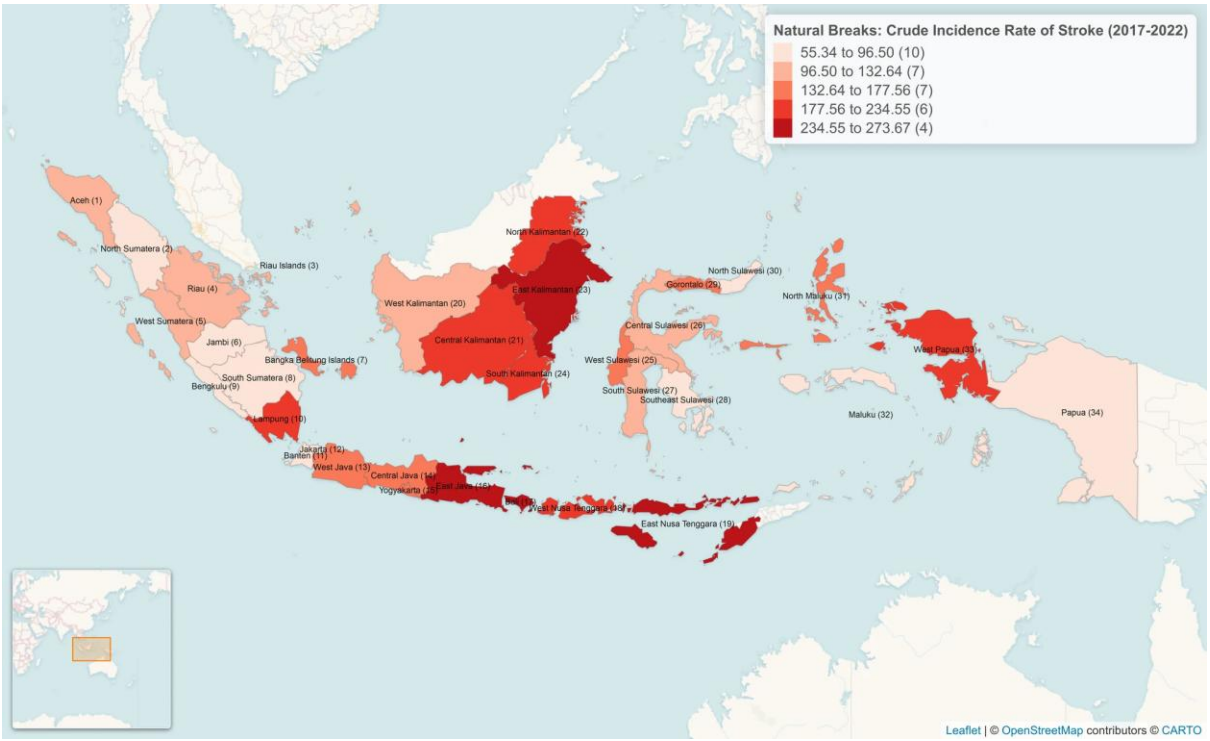


Figure 3 – Stroke incidence across Indonesia [1].

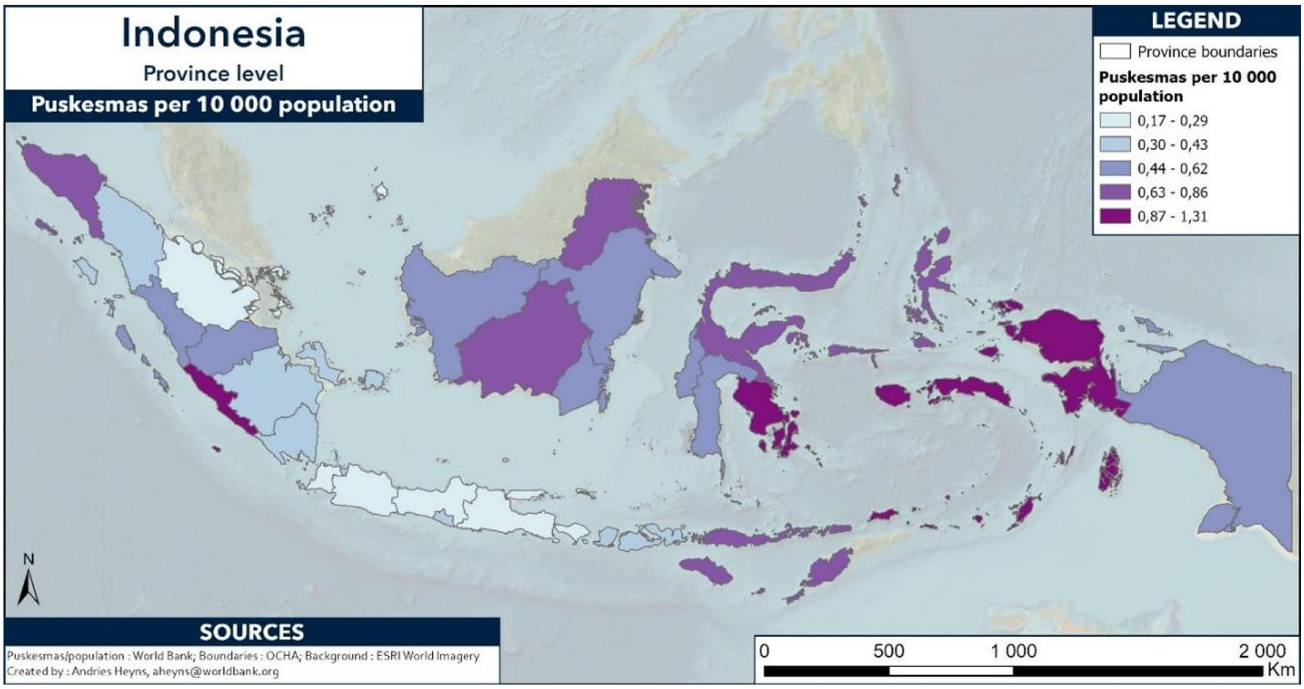
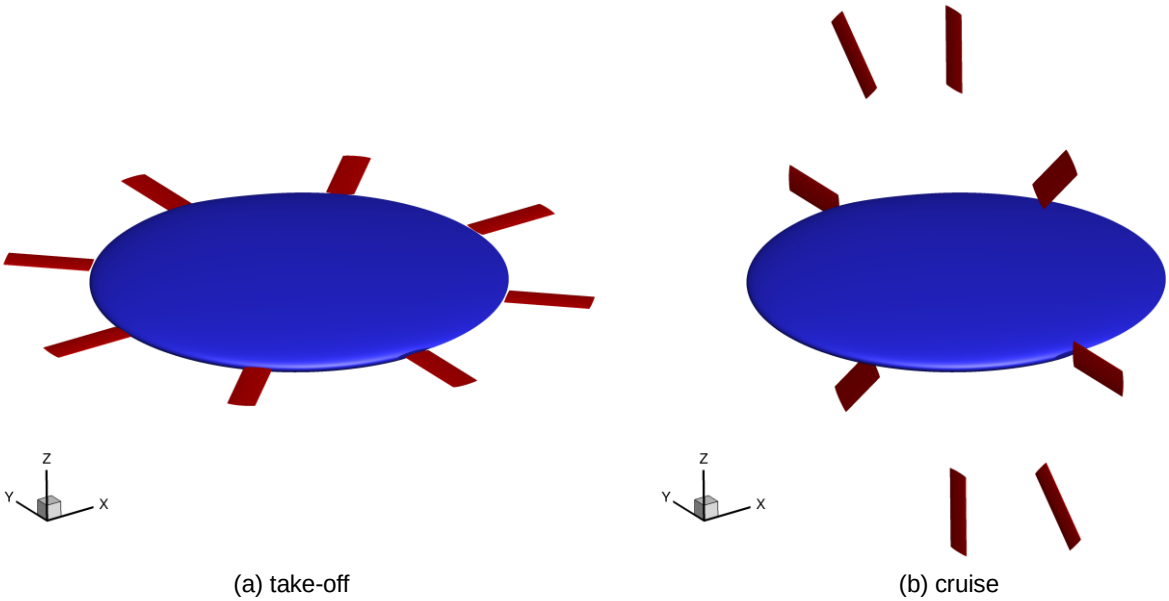


Figure 4 – Map of Community Health Centers per 10,000 Population [4].

4. Configuration

The configuration to be analyzed consists of a fuselage and rotor blades[1] as illustrated in Figure 5. The initial number of blades is set to be three. The analysis is distinguished into two flight modes, hover and cruise, both at sea level consistent with the mission set in the previous section. During the analysis, the fuselage and the rotor blades are treated in isolated domains. Their mutual interaction is excluded from the analysis. All analyses of the rotor blades were performed for an axial flow perpendicular to the rotational plane. This approach allows a steady-state flow analysis in the inertial frame of reference for the fuselage in cruise, and a steady-state flow analysis in a rotating frame of reference for the rotor blades in both hover and cruise, using CFD at NLR described in Section 5. It should be noted that the transitional flight model in a VTOL scenario, where the flow is inherently unsteady, is outside the scope of the present analysis.



(a) take-off (b) cruise

Figure 5 – Configuration of a fuselage and rotor blades.

[1] The wing is discarded for simplicity, anticipating that the lift to be generated by the fuselage will be sufficient.

4.1 Selection of the Rotor Blade

An early high-speed propeller described in a NACA report [5] is chosen for the swivel rotor, where

- the chord is constant along the span with the same family of airfoil NACA-16 series,
- the geometry and experimental data have been digitized and published in a NASA report [6].

A schematic of the propeller test is given in Figure 6, where the hub diameter and the propeller tip diameter are shown to be 32-inch and 9.75-foot, respectively. The 3-bladed propeller is tested in the Langley 16-foot transonic wind tunnel, as illustrated in a photo in Figure 7.

The tip radius of the blade serves as a fundamental parameter in the construction of a swivel rotor configuration. A multiplication factor of the tip radius sets the location of the tip, to which the whole blade geometry is translated, without scaling, keeping the same blade span and cross-sectional airfoil shape. A new radius of the rotor hub follows the new location of the blade. In the analysis presented in this paper, a factor of three is selected following the fuselage sizing. This also yields a considerable change from the conventional blade, that is suitable for the present study. With this factor, the blade diameter becomes 29.25-foot.

It is essential to maintain the same tip speed, which means that the rotational speed must be reduced three times lower. Assuming the twist distribution of the original (conventional) blade was determined to obtain an optimum angle of incidence along the leading edge, the new blade must be retwisted such that the same angle of incidence is maintained along the leading edge. The new twist distribution is shown in Figure 8 (a) compared with the original one, where ξ denotes the normalized distance from the hub towards the tip. In a top (radial) view presented in Figure 8 (b), the tips coincide with each other at $\xi = 1$, while the hub profile shows the difference of twist at $\xi = 0.27$. Bringing the blade to a location with a large radius has the impact that the incoming flow to the blade has become almost uniform.

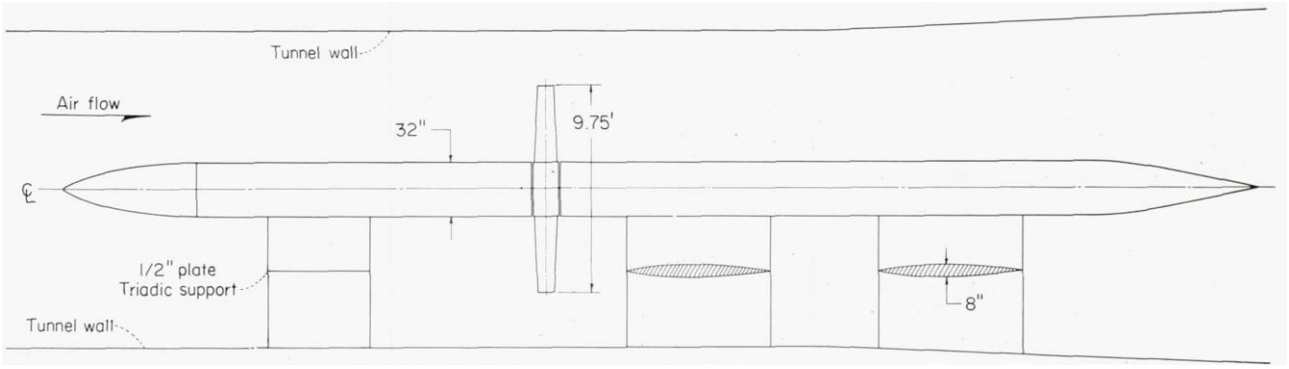


Figure 6 – The propeller test stand with a 9.75-foot tip diameter on a 32-inch hub diameter [5].

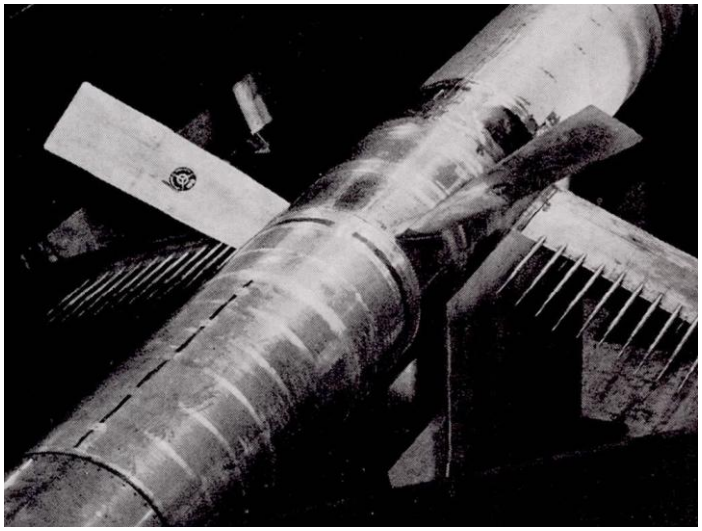
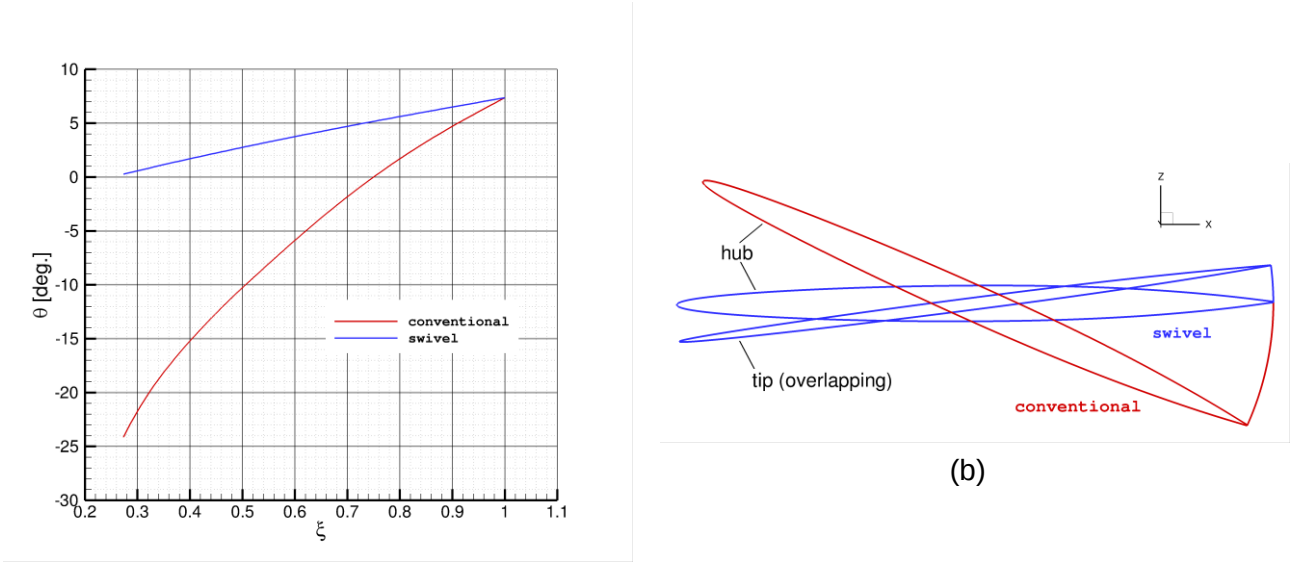


Figure 7 – Propeller in the Langley 16-foot transonic tunnel test section [5].



(a) (b)

Figure 8 – Redistribution of the twist for the swivel rotor.

4.2 Fuselage Sizing and Profile Selection

The fuselage cross section is given an airfoil shape in order to generate lift. The chord of the fuselage on the symmetry plane follows the payload volume and is consistent with the multiplication factor of the tip radius of the rotor blades, described in the previous section. With a small gap between the fuselage and the rotor, the fuselage chord has a value approximately equal to the rotor blade tip diameter subtracted by the blade span. A thick 14% supercritical airfoil NASA SC(2)-0714 was initially considered, but it cannot accommodate the specified cylindrical volume. The thickness had to be increased by modifying both the upper and lower surface to become a 15% thick variant of the airfoil.

4.3 Generation of the Geometries

The geometry of the fuselage and rotor blades are treated in the same way in a parametric domain. The geometry is described parametrically in terms of airfoils and planform properties. The fuselage is treated as a wing-like geometry defined by a distribution of the airfoil shape, chord, twist, sweep and dihedral from the symmetry plane to the tip, as illustrated in Figure 9. In this respect, the circular planform of the fuselage shown is just a simple choice.

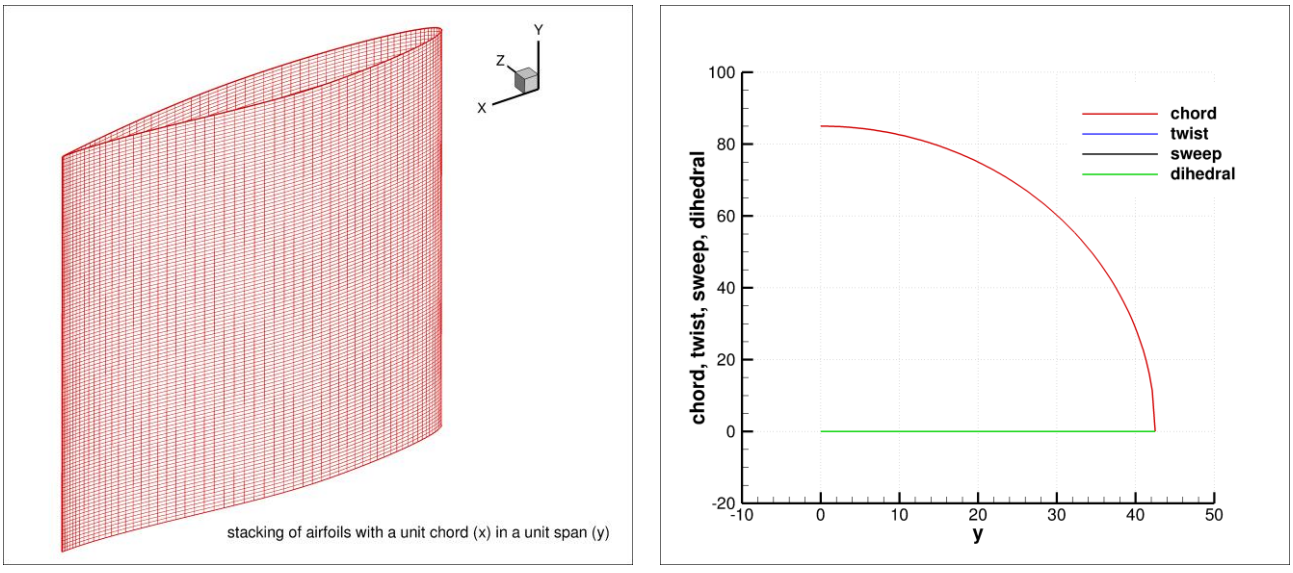


Figure 9 – Parametric representation of the fuselage from the symmetry plane to the tip.

5. Computational Fluid Dynamics (CFD) Method

The CFD simulations for the present analysis were performed using ENFLOW, a high-fidelity CFD code developed in-house at NLR [7]. ENFLOW has been used extensively in various European Projects, amongst others concerning complex rotating configurations, e.g. [8], [9]. It solves the time-dependent Reynolds-Averaged Navier-Stokes (RANS) equations in multi-block structured grids. The two-equation Menter SST turbulence model is used to close the equations.

Ffowcs Williams and Hawkings (FWH) analogy [12] is used to determine tonal acoustic characteristics of the rotating blades, which consists of thickness and loading noise. The thickness contribution is due to the motion of the geometry only. The loading contribution is due to the surface pressure computed by the CFD simulation. The noise analysis is performed in a post-processing fashion after the CFD analysis.

6. Effects of Radial Translation of the Blades

First, a comparison of the experimental data [6] and CFD simulation results was made for a selected data set, where the rotational speed is kept fixed at 1600 rpm and the Mach number is varied to give a range of the advance ratio, J. Three blade pitch angles are selected, $\beta = 40.2$, 45.4, 50.8 for the comparison. Figure 10 shows a reasonably good agreement between the experimental data and CFD numerical results in terms of the polar curve of power (C_P) versus thrust (C_T) coefficients, both in a 3-blade conventional configuration.

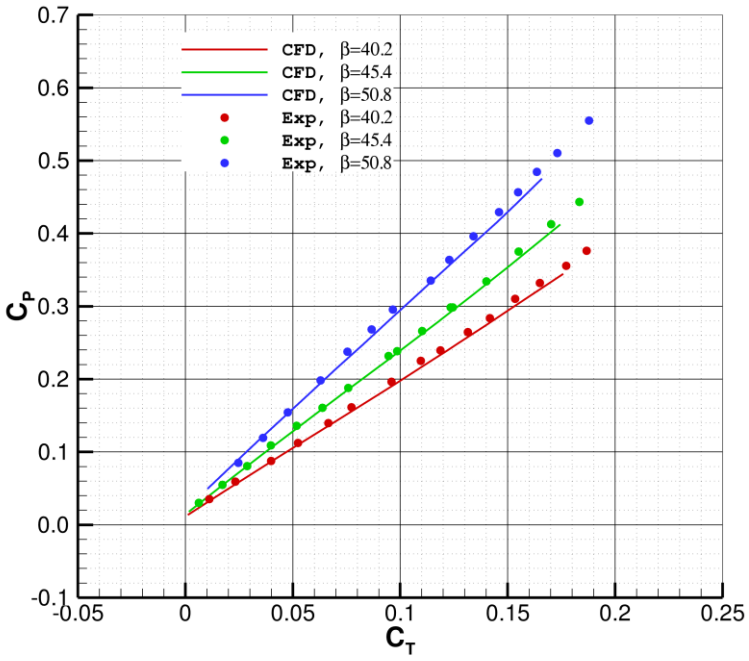


Figure 10 – Comparison of experimental data and CFD numerical results.

As described previously, a multiplication factor of three is used to translate the blade radially to a location with a large radius in order to construct a swivel configuration, with the necessary retwisting, and lowering of the rotational speed to one-third of 1600 rpm, i.e. 533 rpm. The impact in terms of power and thrust can be seen in Figure 11 as function of advance ratio J. The swivel configuration shifts the operation to a higher thrust and power in the same range of J. At lower advance ratios the rotor blades eventually stall. However, an observation of the flow on the rotor blades in the conventional configuration reveals that the flow has also separated, although it does not seem to be the case from the thrust curve.

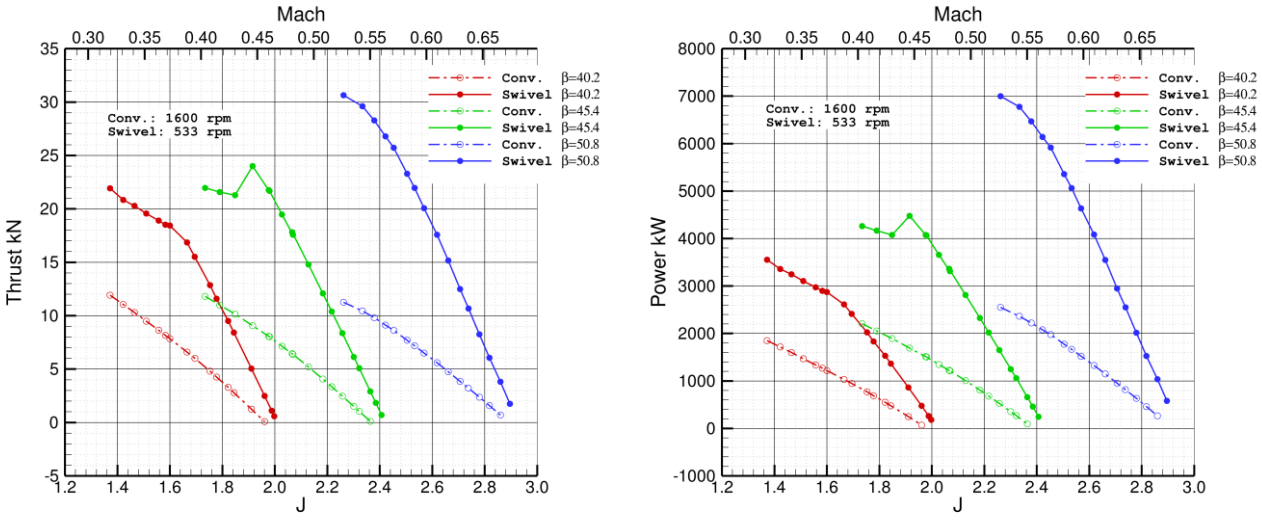


Figure 11 – Impact of a large tip radius to thrust and power.

Figure 12 presents the efficiency curves, demonstrating that the swivel configuration delivers a significantly higher efficiency. This higher efficiency can be attributed to the more uniform flow and favorable distribution of angle of incidence due to the retwisting. In the low advance ratio regimes, the efficiency curves indicate that the swivel configuration has a worse stall situation as indicated by the thrust curves. Interestingly, a search of the literature revealed an early work of Bolonkin [11], where a rotor is placed on a ring around a fuselage ("fusefan"), a similar situation with a large distance from the center of rotation, leading to an increase in efficiency.

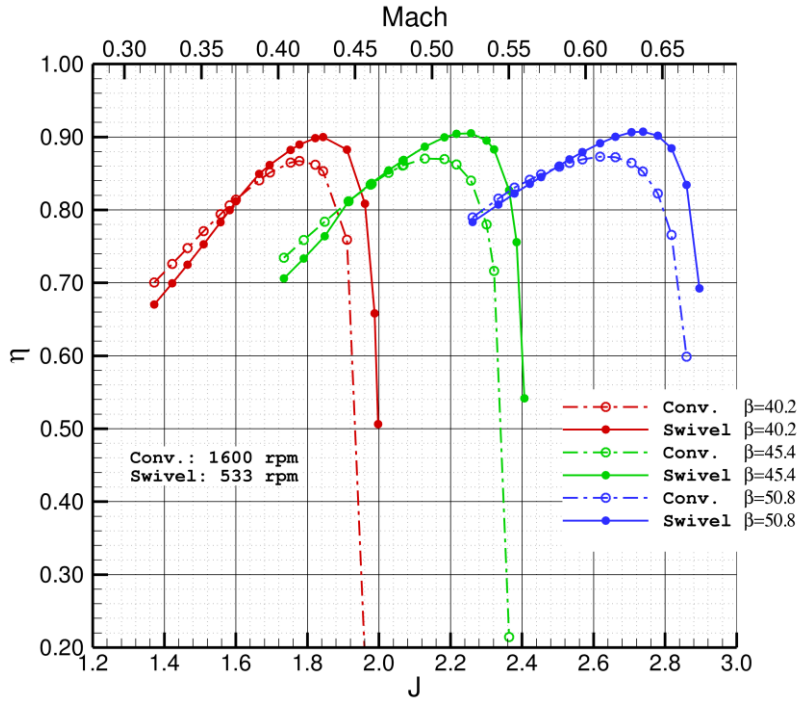


Figure 12 – Impact of a large tip radius to efficiency.

Although no experimental data is available for the static condition, it is instructive to see the impact of a large tip radius at a hover condition with different rotational speeds and blade pitch angle. Figure 13 shows that the large tip radius has the effect to significantly increase the slope of the thrust curve with respect to the blade pitch. It is observed that the flow at the blade pitch of 10 degrees has started to separate in all cases.

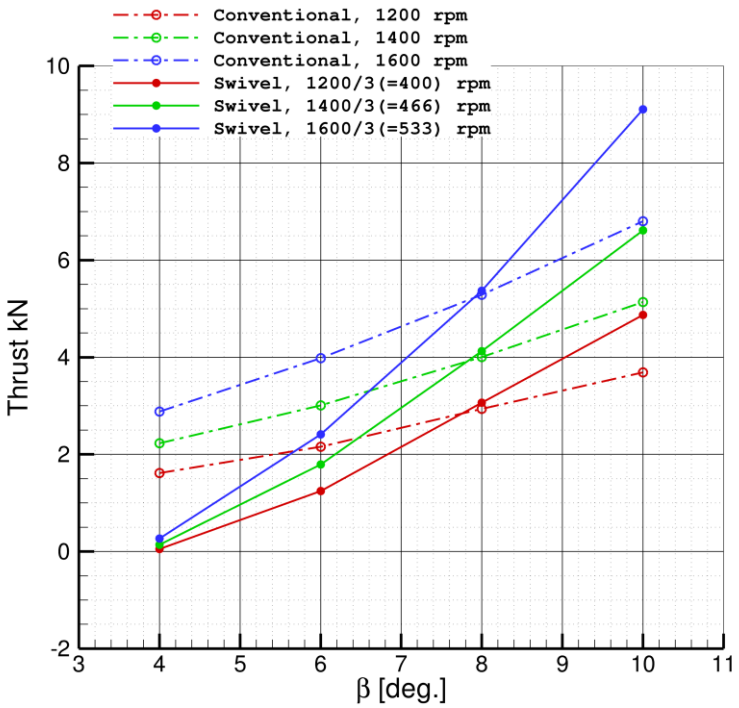


Figure 13 – Impact of a large tip radius at hover with different rotational speeds.

The NACA-16 profile has a rather small leading edge radius that is prone to stall at a hover condition. In order to improve the situation, an optimization has been performed with the objective to minimize power. A fixed thrust level at 8 degrees angle of blade pitch was taken as a representative design condition, where the flow is still fully attached on the surface. Geometrical inequality constraints were applied, where the leading edge radius and the cross-sectional area of the airfoil are not allowed to get smaller than their initial values. A gradient-based optimization with an adjoint solver developed at NLR [10] was used for the optimization. Figure 14 presents the optimization history where the power has finally been reduced significantly. It has been verified that the new (optimized) geometry has delayed the stall to a higher blade pitch angle.

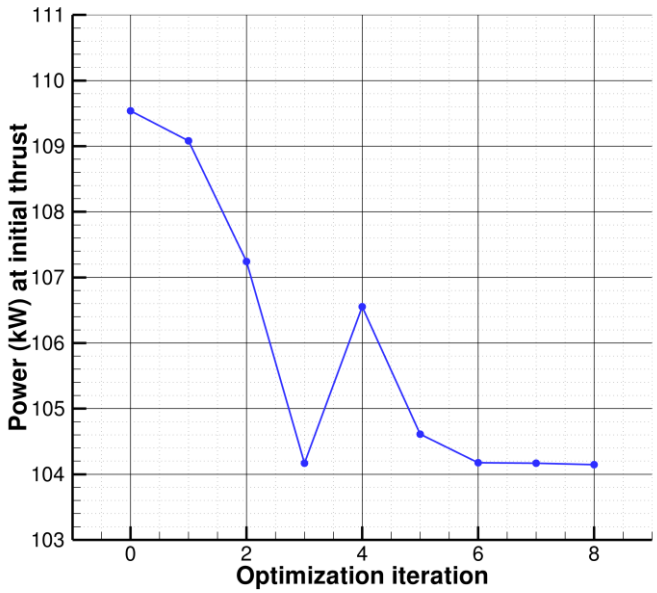
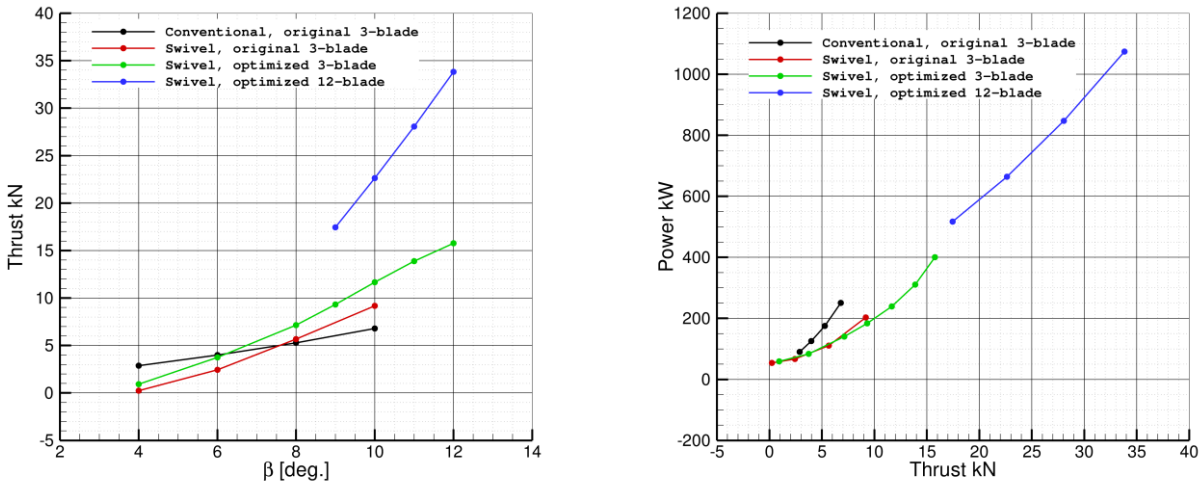


Figure 14 – Constrained optimization of the rotor blade to improve stall condition.

7. Design for Purpose of the Swivel Configuration

7.1 Hover

In hover, the rotor blades are required to produce a thrust to carry the maximum take-off weight (MTOW), consisting of a payload of 200 kg (≈ 2 kN weight) and all the structure and system, plus an additional thrust to enable maneuvers and acceleration during the transitional flight mode towards cruise. For a new aircraft architecture there is no statistics available to estimate the structural and system requirements. Nevertheless, a thrust of 12 kN to balance MTOW and another 12 kN for maneuvers and transitional flight mode are assumed, setting a total of 24 kN required to be available during the hover flight mode.



(a) (b)

Figure 15 – Thrust and power at hover at different angles of blade pitch.

Figure 15 presents a summary from the original 3-blade rotor in a conventional configuration to the optimized 12-blade rotor in a swivel configuration. It is clear that the original 3-blade conventional configuration cannot meet the target thrust of 24 kN. The swivel configuration increases the thrust at a higher blade pitch, but still is not able to meet the target. The optimized blade gives a significant improvement, delaying the stall to a significantly higher thrust, but it falls short of meeting the target.

One may start looking at the possibility of increasing the blade count, considering that the swivel configuration offers versatility in this respect. A large step change in the blade count is chosen, from originally 3 to 12, anticipating that the thrust will not increase linearly with the blade counts. The new blade counts delivers a thrust that exceeds the target level in a range of blade pitch between 10 to 12 degrees as shown in Figure 15 (a). Of course, as anticipated, this high thrust capability comes with a cost of high power regimes, indicated in Figure 15 (b).

7.2 Cruise

At cruise, the capability of the fuselage to carry the weight must be investigated first. Again, a rather conservative approach is taken in specifying the requirement. The aircraft must also pass a phase of deceleration from cruise to a transitional flight mode and ultimately to hover and landing. The load must be transferred in full from the fuselage to the rotor blade. It should be noted that because of the specified mission to fly at sea level, there is not much room to adjust the altitude during this phase.

Figure 16 shows the pressure distribution on the symmetry plane and on the surface of the fuselage at a flight speed of about 480 km/h at sea level at zero angle of attack. Figure 17 demonstrates that the fuselage with the current choice of airfoil and planform gives an ample lift capability to carry the weight. A higher lift capability is demonstrated at a slightly higher angle of attack of 1 degree. By virtue of the low aspect ratio planform, the lift-to-drag ratio is rather poor, below 10, which can be expected.

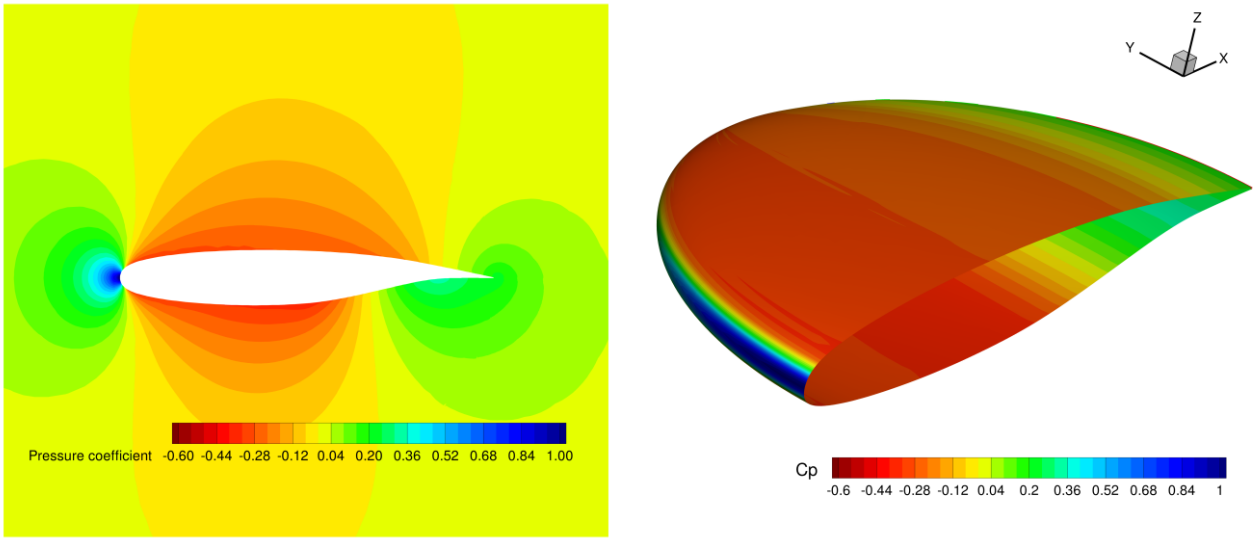
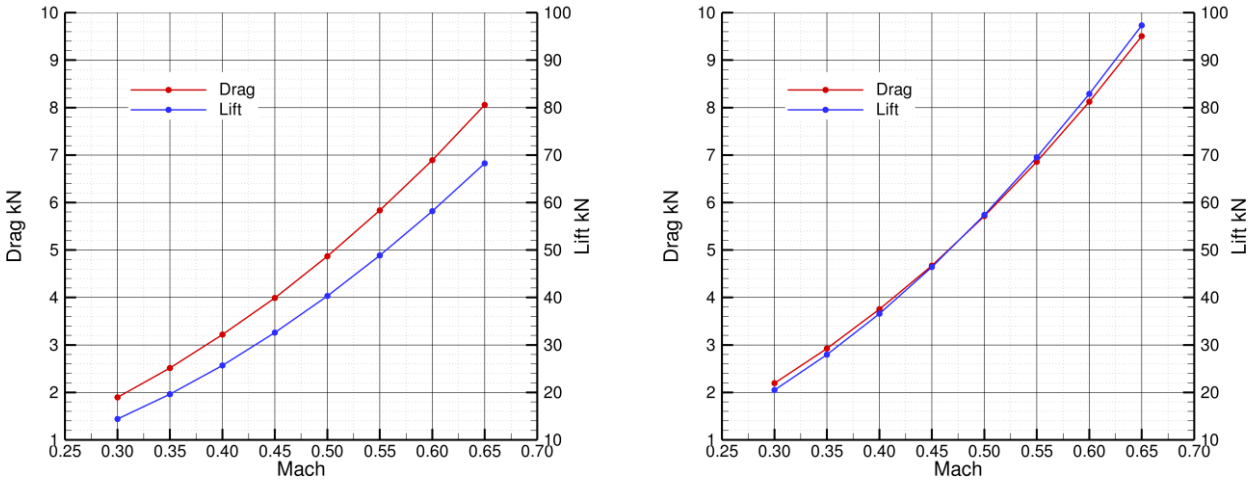


Figure 16 – Pressure coefficient (Cp) distribution on the symmetry plane and on the surface of the fuselage at $M = 0.4$ and $\alpha = 0$ deg.



$\alpha = 0$ $\alpha = 1$

Figure 17 – Lift and drag curves with varying Mach number at angles of attack of 1 and 2 degrees.

7.3 Coupling Hover and Cruise

While the fuselage can offer a high lift capability, the limiting factor at cruise is the power required by the 12 rotor blades to counter the drag. A range of Mach numbers is selected from 0.35 to 0.50, and the corresponding drag of the fuselage is passed on as a target thrust to the simulation of the rotor blades. During the simulation, the blade pitch is trimmed iteratively to achieve the target thrust, and its corresponding power determines the capability of the rotor blades to fly steadily at cruise.

The hover and cruise flight conditions are now connected in terms of power required and weight capability in Figure 18. The term weight capability in the context of hover is equivalent with thrust capability of the rotor blades, while in the context of cruise it is equivalent with lift capability of the fuselage. This is the initial (preliminary) first picture for the assessment of the swivel configuration. For the estimated weight of 12 kN, in a steady hover flight, extrapolating the red curve to the left, the power required would need about 400 kW. But in a steady cruise flight for the same weight, although the current choice of the geometry offers a high lift capability, the curve indicates an oversized planform area that still needs an iteration, that is to achieve an efficient performance at a moderately high speed of Mach 0.4.

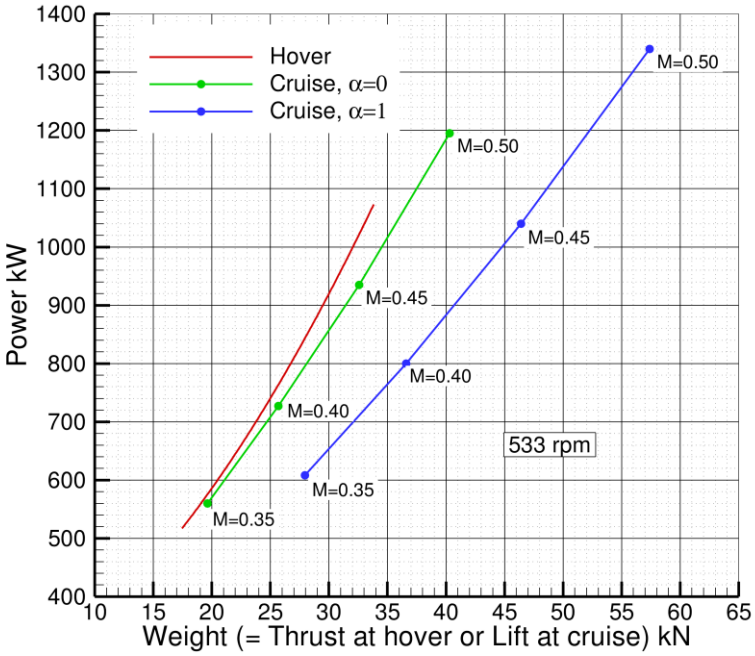


Figure 18 – Hover and cruise initial matching curves.

8. Noise Assessment

The Ffowcs Williams and Hawkings (FWH) analogy is used to determine the noise at an observer located in a radial distance of 15 times the tip radius from the tip. Figure 19 shows a large potential to reduce noise, where a reduction of almost 10 dB for the same thrust can be achieved by transforming a conventional configuration to a swivel one.

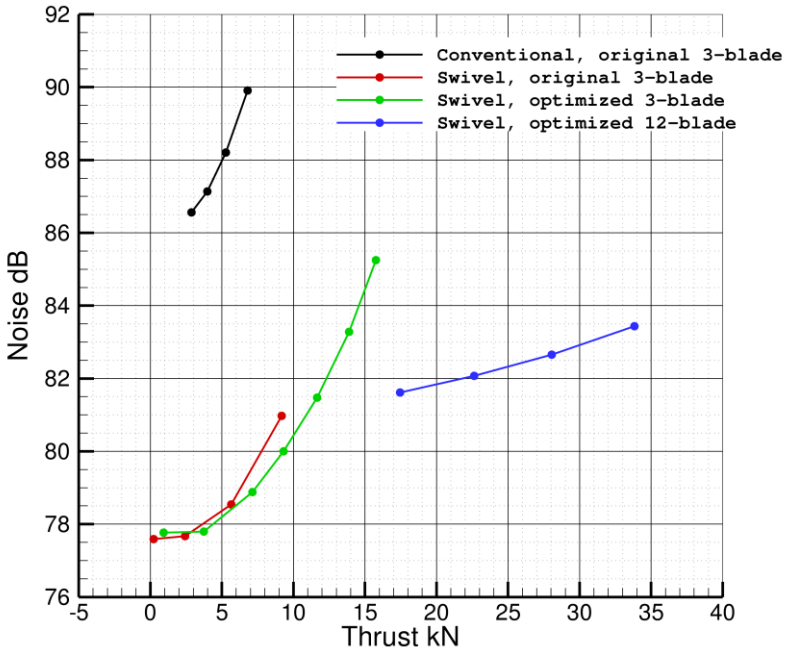


Figure 19 – Impact of swivel configuration to noise.

9. Conclusions

A preliminary feasibility study of the novel swivel rotor architecture has been presented by means of a specific hypothetical but relevant use-case. It has revealed significant promising benefits in terms of propulsive efficiency and noise. For the use-case under consideration, the analysis indicates that a high-speed high-lift drone utilizing a swivel rotor propulsion is aerodynamically feasible for hover and cruise conditions, but another iteration for the fuselage is still needed to ensure an efficient cruise operation. Further research needs to be done to have a better understanding of the design space of the swivel configuration, including system constraints such as powertrain, stability and control, transitional flight mode, etc. possibly by means of a model-scale prototype.

Contact Author Email Address

mailto: bambang.soemarwoto@nlr.nl

Copyright Statement

The authors confirm that they, and/or their company or organization, hold copyright on all of the original material included in this paper. The authors also confirm that they have obtained permission, from the copyright holder of any third-party material included in this paper, to publish it as part of their paper. The authors confirm that they give permission, or have obtained permission from the copyright holder of this paper, for the publication and distribution of this paper as part of the ICAS proceedings or as individual off-prints from the proceedings.

References

[1] Zainuddin A.A., Kadir, R.R.A., Kuswanto, H. *et al.* The major risk factor of stroke across Indonesia; a nationwide geospatial analysis of universal health coverage program. *Arch Public Health* 83, 169, 2025.

[2] O'Reilly, T., Börnert, P., Liu, H. *et al.* 3D magnetic resonance fingerprinting on a low-field 50 mT point-of-care system prototype: evaluation of muscle and lipid relaxation time mapping and comparison with standard techniques. *Magn Reson Mater Phy* 36, 499–512, 2023.

[3] Rudiarto, I., Handayani, W. and Sih Setyono, J. A Regional Perspective on Urbanization and Climate-Related Disasters in the Northern Coastal Region of Central Java, Indonesia. *Land 7*, 34, 2018.

[4] Bosch, L., Heyns, A. and Debebe. Z. Health Care Access Come Rain or Shine: A Multifactorial Accessibility Study of Public Primary Health Care in Indonesia. Washington DC: World Bank, 2025.

[5] Evans, J.A. and Liner, G.A. Wind Tunnel Investigation of the Aerodynamic Characteristics of a Full-Scale Supersonic-Type Three-Bladed Propeller at Mach Numbers to 0.96, NACA Technical Report 1375, 1958.

[6] Harris, F.D., Performance Analysis of Two Early NACA High Speed Propellers with Application to Civil Tiltrotor Configurations, NASA Contractor Report 196702, 1996.

[7] Kok, J.C. A high-order low-dispersion symmetry-preserving finite-volume method for compressible flow on curvilinear grids, *Journal of Computational Physics*, 228, 6811-6832, 2009.

[8] Meheut, M., Sartor, F., Vergez, M., Laban, M., Schnell, R., Stuermer, A.W., and Lefevre, G., Assessment of Fan/Airframe aerodynamic performance using 360° URANS computations: Code-to-Code comparison between ONERA, DLR, NLR and Airbus, *AIAA Paper 2019-0582*, 2019.

[9] Stokkermans, T., Veldhuis, L., Soemarwoto, B., Fukari, R. and Eglin, P., Breakdown of aerodynamic interactions for the lateral rotors on a compound helicopter, *Aerospace Science and Technology*, Vol. 101, June 2020.

[10] Soemarwoto, B., van der Ven, H., Kok, J.C., and Janssen, S.R. Unsteady Adjoint Method for Aeroacoustic Propeller Optimization, *AIAA Paper 2021-3054*, 2021.

[11] Bolonkin, A. A High Efficiency Fuselage Propeller ("Fusefan") for Subsonic Aircraft, *SAE Paper 1999-01-5569*, 1999.

[12] Ffowcs Williams, J.E. and Hawkings, D.L. Sound Generated By Turbulence And Surfaces In Arbitrary Motion,*Philosophical Transactions of the Royal Society A*, 264, 321–342, 1969.